Simultaneous Angle-of-Arrival and Frequency Measurement System Based on Microwave Photonics

Jiewen Ding, Dan Zhu, *Member, IEEE,* Yue Yang, Boyang Ni, Chao Zhang and Shilong Pan, *Senior Member, IEEE, Fellow, OSA*

***Abstract*—A simultaneous angle-of-arrival (AOA) and frequency measurement system based on microwave photonics is proposed and experimentally demonstrated. The measurement of the AOA and the frequency is realized based on the simultaneous AOA-to-power and frequency-to-time mapping. Using optical pulses and optical dispersion elements, the frequencies of the received RF signals will map to the time intervals of the output electrical pulses. At the same time, by introducing a DPMZM, the received RF signals with the AOA-dependent phase differences interfere in the optical domain, mapping the AOA-dependent phase difference to the power of the interfered optical sidebands, which further maps to the output electrical pulse amplitudes. By measuring the time intervals and the normalized amplitudes of the output electrical pulses, the AOA and the frequency can be obtained simultaneously. In addition, the measurement of multiple RF signals can be realized due to the independence of the output mapping signals in the time domain for different RF frequencies. A proof-of-concept experiment is carried out. The AOA measurement from -70° to 70° with a measurement error of ±2.5°, and the frequency measurement from 5 to 15 GHz with a measurement error of ±12 MHz are successfully achieved simultaneously. The measurements of single-tone and multiple RF signals are experimentally achieved.**

***Index Terms*—Microwave photonics, angle-of-arrival measurement, frequency measurement, frequency-to-time mapping.**

I. Introduction

ANGLE-of-arrival (AOA) measurement is used to determine the azimuth of a microwave signal and realize the localization of microwave sources [1]. Due to its wide applications in wireless communication, radar, and electronic warfare systems [2-4], the AOA measurement has recently been a research hotspot. There are two main types of AOA measurement methods for traditional electronic systems. One is the amplitude-comparison method, for which the AOA information is obtained by comparing the power of the received signal at different angles on the antenna's main axis [5]. The structure of this method is simple, and the measurement speed is fast. However, a high measurement accuracy requires a narrow antenna beam width, while a wide AOA measurement range needs a wide antenna beam width. A trade-off between measurement accuracy and range exists. To solve this problem, the phase-comparison method has been developed [6, 7]. Two or more antennas are introduced to receive the RF signals. In the far-field scenario, there are phase differences between the RF signals received by different antennas, when the wavefront is not parallel to the antenna baseline. The AOA can be measured by detecting the phase differences between the received RF signals. Traditionally, the phase difference can be obtained in the digital domain after the analog-to-digital converters (ADCs). With the RF systems developing towards high frequency and wide bandwidth, great challenges exist with the ADCs and the amount of data to be processed.

Microwave photonic AOA measurement methods have been proposed due to photonics' wide working bandwidth and parallel signal processing capability [8-10]. To avoid the requirement of high sampling rate, AOA measurement based on photonic down-conversion is proposed [11-19]. The key point is to down-convert the received RF signals to the intermediate frequency (IF) band with a LO signal based on microwave photonic approaches. Then the IF signals can be converted into the digital domain by using ADCs with low sampling rates. After discrete Fourier transformation of the IF signals, the AOA and the frequency of the received signals can be estimated from the phase and amplitude spectrums, respectively. Furthermore, to achieve the measurements with multiple RF signals in a large bandwidth, AOA measurement based on a photonic scanning receiver [17, 18] or a channelized receiver [19] is proposed, respectively. The critical point is using a frequency-stepped LO signal [17, 18] or multiple LO signals [19] to replace the LO signal with a fixed frequency. In this way, the frequency down-conversion and the AOA measurements for multiple RF signals are achieved. However, for these methods, the realization of the multiple RF signals in a wideband depends on increasing the system complexity or the requirement of devices. For example, the method based on the channelized receiver needs to add extra channels (optical links) to measure multiple RF signals over a wide bandwidth.

In [20, 21], a coherent optical processing method is proposed

Manuscript received xx, xxxx. This work was supported in part by National Natural Science Foundation of China under Grant 61971222, and in part by the Natural Science Foundation of Jiangsu Province under Grant BK20220076. (Corresponding author: Dan Zhu.)

The authors are with College of Electronic and Information Engineering, Nanjing University of Aeronautics and Astronautics, Nanjing 210016, China (e-mail: danzhu@nuaa.edu.cn).

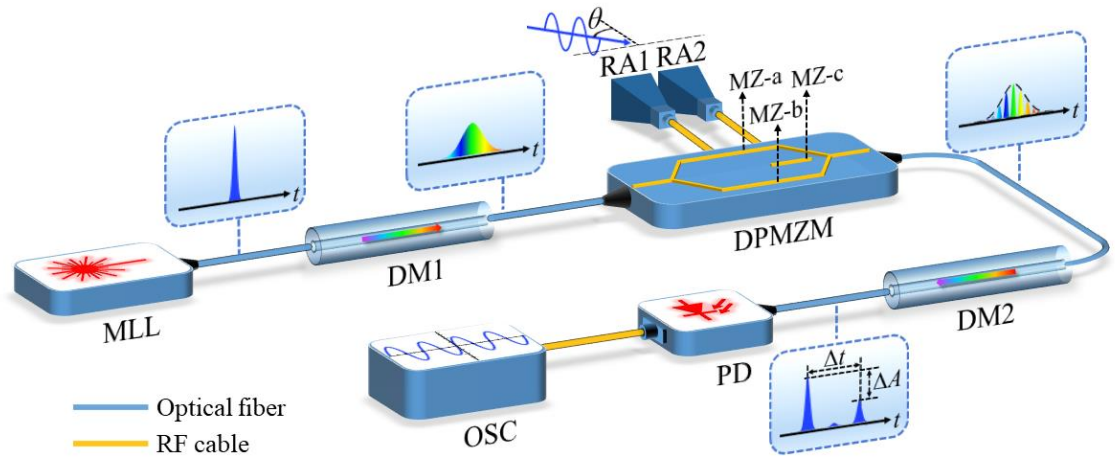

Fig. 1. The schematic diagram of the proposed simultaneous AOA and frequency measurement system based on microwave photonics. MLL: mode-lock laser; DM: dispersive media; RA: receive antenna; DPMZM: dual-parallel Mach-Zehnder modulator; PD: photodetector; OSC: oscilloscope.

to realize the AOA and frequency measurement. By introducing unequal lengths of fibers, random time delays are introduced to the RF signals received by the antenna array. The outputs of these fibers contain correlations among the received RF signals with various time delays. Hence, the interference beams captured by a charge-coupled device (CCD) can be used to reconstruct the AOA and the frequency of the received RF signals. The frequency measurement within the range of 12-18 GHz, and the AOA measurement within the range of ±15º are experimentally achieved. However, sophisticated algorithms are needed to reconstruct the AOA and the frequency, which is time-consuming. In addition, this system contains large-scale photonic links and optical space links, which makes it bulky and complex.

To get a streamlined structure and a fast measurement speed, AOA measurement based on the AOA-to-power mapping is studied [22-31]. Two received RF signals with the AOA-dependent phase difference are converted to the optical domain through the cascaded [22-24] or parallel [25-27] electro-optic modulators, which will interfere in the optical domain. The AOA-dependent phase difference will map to the power of the interfered optical sidebands. Thus, the AOA can be obtained by measuring the power of the interfered optical sidebands. Furthermore, in [28], through the optical-to-electrical conversion, the AOA-dependent phase difference can be mapped into the DC power in the electrical outputs, which can be detected easily. To expand the AOA measurement range, a two-level electrical signal is applied to control the transmission point of the dual-drive Mach-Zehnder modulators (DDMZM) in [29]. This way, two asymmetric AOA-to-power mapping curves are obtained to eliminate the measurement ambiguity, and the AOA measurement range will be improved. In [30, 31], the parallel DDMZMs are used to output two different DC powers simultaneously. By estimating the AOA from the ratio of the two DC powers, the measurement ambiguity caused by the amplitude of the received RF signal can be eliminated. However, for the current AOA-to-power mapping approaches, the AOA estimated from the AOA-dependent phase difference is related to the frequency of the received RF signal. Hence, an additional frequency measurement approach is needed to obtain the frequency of the received RF signal. In addition, it is difficult to achieve the measurement of multiple RF signals, since the AOA values of the multiple RF signals will all map to the DC power and can't be distinguished.

In this paper, a simultaneous AOA and frequency measurement system based on AOA-to-power and frequency-to-time mapping is proposed and demonstrated. The optical pulses generated from a mode-lock laser (MLL) are injected into a linearly chirped fiber Bragg grating (LCFBG). The output chirped optical pulses are modulated by the received RF signals with the AOA-dependent phase difference through a dual-parallel Mach-Zehnder modulator (DPMZM). Another LCFBG with an inverse-matched dispersion is used to compress the modulated optical pulses in the time domain. After the optical-to-electrical conversion, frequency-to-time mapping is achieved. For each frequency component of the RF signal, the output electrical signal consists of two pulses with a time interval proportional to the RF frequency. Meanwhile, by introducing the DPMZM, the AOA-dependent phase difference will map to the power of the interfered optical sidebands and further map to the amplitude of the output electrical pulses.

In this way, simultaneous AOA-to-power and frequency-to-time mapping are achieved. Thus, the AOA and the frequency of the received RF signals can be simultaneously estimated based on the amplitude and the time interval of the output electrical signals, respectively. In addition, due to the independence of the output mapping signals in the time domain for different RF frequencies, the measurement of multiple RF signals can also be achieved. Theoretical analyses and simulations are carried out. A proof-of-concept experiment is taken. Both the measurements of single-tone and multiple RF signals are taken. The AOA measurement from -70º to 70º, and the frequency measurement from 5-15 GHz are simultaneously achieved. The AOA measurement error is within ±2.5º, while the frequency measurement error is within ±12 MHz. As compared with the approaches based on microwave photonic down-conversion, microwave photonic channelization, and the coherent optical processing, the proposed system can realize a

wider AOA and frequency measurement range. Meanwhile, the proposed system can achieve simultaneous AOA and frequency measurement with multiple signals. Besides, there is no need for large-scale photonic links and space optical links, greatly reducing the complexity and cost of the system.

II. Principle

The schematic diagram of the proposed simultaneous AOA and frequency measurement system is shown in Fig. 1. The optical pulse generated by the MLL has a Gaussian shape. Mathematically, the envelope of the optical pulse is as follows

$$U_1(0,t)=\exp\left(-\frac{t^2}{2T_0}\right) \tag{1}$$

where T_0 is the full width at half maximum (FWHM) of the optical pulse. The optical pulses are then injected into the dispersive media (DM, DM1) with the 2nd dispersion value of $\beta_2 z$, which are then stretched in the time domain. Based on the Schrodinger equation [32], the output of DM1 is as follows

$$\begin{aligned}U_2(z,t)&=\frac{T_0}{\left(T_0^2-j\beta_2 z\right)^{1/2}}\exp\left[-\frac{t^2}{2\left(T_0^2-j\beta_2 z\right)}\right]\\&=\underbrace{\frac{1}{\left[1+\left(\frac{z}{L_D}\right)^2\right]^{1/4}}\exp\left[-\frac{t^2}{2T_0^2\left[1+\left(\frac{z}{L_D}\right)^2\right]}\right]}_{|U(z,t)|}\\&\cdot\exp\left[-j\frac{\operatorname{sgn}(\beta_2)\frac{z}{L_D}}{2T_0^2\left[1+\left(\frac{z}{L_D}\right)^2\right]}t^2+\frac{j}{2}\arctan\left(\operatorname{sgn}(\beta_2)\frac{z}{L_D}\right)\right]\end{aligned} \tag{2}$$

where $L_D=T_0^2/|\beta_2|$. As can be seen, the envelope of the time-stretched signal $|U(z,t)|$ also has the Gaussian shape, but the FWHM changes from T_0 to $T_1=T_0[1+(z/L_D)^2]^{1/2}$. T_1 is equivalent to the sampling duration of the Fourier transform. Therefore, the frequency resolution of the proposed system can be defined as $1/T_1$, which is proportional to the FWHM T_0 and the 2nd dispersion value of $\beta_2 z$. This also indicates that the original non-chirped optical pulse becomes a chirped one after passing through DM1. It is assumed that $A=1/[1+(z/L_D)^2]^{1/4}$ and $C=1+j\operatorname{sgn}(\beta_2)z/L_D$, then Eq. (2) can be rewritten as follows

$$U_2(z,t)=A\exp\left[-\frac{Ct^2}{2T_1^2}\right]\exp\left[\frac{j}{2}\arctan\left(\operatorname{sgn}(\beta_2)\frac{z}{L_D}\right)\right] \tag{3}$$

The RF signals are received by two receive antennas (RAs) with a distance of d. As shown in Fig. 1(c), due to the AOA, there is a time delay τ, and a corresponding phase difference φ, between the RF signals received by RA1 and RA2, and the corresponding expressions are as follows

$$\begin{cases}\tau=\dfrac{d\sin(\theta)}{\mathrm{c}}\\ \varphi=\dfrac{2\pi\mathrm{c}\,\tau}{\lambda}=\dfrac{2\pi d\sin(\theta)}{\lambda}\end{cases} \tag{4}$$

where θ represents the AOA, c is the speed of light in vacuum, and λ is the wavelength of the received RF signals. To avoid measurement ambiguity, d is set to be equal to $\lambda/2$, thus $\varphi=\pi\sin(\theta)$. Mathematically, the two received RF signals can be expressed as follows

$$\begin{cases}s_1=V_{\mathrm{RF}}\cos(\omega_{\mathrm{RF}}t)\\ s_2=V_{\mathrm{RF}}\cos(\omega_{\mathrm{RF}}t+\varphi)\end{cases} \tag{5}$$

where V_{RF} and ω_{RF} are the amplitude and the angular frequency of the received RF signals, respectively. The two received RF signals are fed into the two sub-MZMs (MZM-a and MZM-b) of the DPMZM, respectively. Both the two sub-MZMs are biased at the minimum transmission point. Considering the small signal modulation condition, the higher-order optical sidebands can be ignored. The optical outputs from the two sub-MZMs are as follows

$$\begin{cases}U_{\text{MZ-a}}(z,t)=\gamma U_2(z,t)J_1(\beta)\\ \qquad\cdot\left[\exp(j\omega_{\mathrm{RF}}t)+\exp(-j\omega_{\mathrm{RF}}t)\right]\\ U_{\text{MZ-b}}(z,t)=\gamma U_2(z,t)J_1(\beta)\\ \qquad\cdot\left[\exp(j\omega_{\mathrm{RF}}t+j\varphi)+\exp(-j\omega_{\mathrm{RF}}t-j\varphi)\right]\end{cases} \tag{6}$$

where γ is the insertion loss of the sub-MZM, $J_1(\cdot)$ is the 1st Bessel function, and $\beta=\pi V_{\mathrm{RF}}/V_\pi$ is the modulation depth. Therefore, the output of the DPMZM is as follows

$$U_3(z,t)=U_{\text{MZ-a}}(z,t)+U_{\text{MZ-b}}(z,t)e^{j\psi} \tag{7}$$

where ψ is the additional phase introduced by MZM-c of the DPMZM. Here MZM-c is biased at the quadrature transmission point. The output of the DPMZM injects into DM2 with the 2nd dispersion value of $-\beta_2 z$. The output of DM2 is as follows

$$\begin{aligned}U_4(z,t)&=\gamma J_1(\beta)\exp\left(-j\frac{\omega_{\mathrm{RF}}^2\beta_2 z}{2}\right)\\&\cdot\left\{\exp\left[-\frac{(t+\omega_{\mathrm{RF}}\beta_2 z)^2}{2T_0^2}\right]\exp(-j\omega_{\mathrm{RF}}t)\right.\\&+\exp\left[-\frac{(t-\omega_{\mathrm{RF}}\beta_2 z)^2}{2T_0^2}\right]\exp[j\omega_{\mathrm{RF}}t]\\&+\exp\left[-\frac{(t+\omega_{\mathrm{RF}}\beta_2 z)^2}{2T_0^2}\right]\exp[-j\omega_{\mathrm{RF}}t+j(\psi-\varphi)]\\&\left.+\exp\left[-\frac{(t-\omega_{\mathrm{RF}}\beta_2 z)^2}{2T_0^2}\right]\exp[j\omega_{\mathrm{RF}}t+j(\varphi+\psi)]\right\}\end{aligned} \tag{8}$$

As can be seen, there are four optical pulses in the output of DM2. In the time domain, two of the optical pulses with phases of 0 and $\varphi+\psi$ respectively are located $\omega_{\mathrm{RF}}\beta_2 z$ to the left of the original optical carrier pulse. Two other optical pulses with phases of 0 and $\psi-\varphi+$ respectively are located $\omega_{\mathrm{RF}}\beta_2$ to the right

of the original optical carrier pulse. It is not difficult to find that the optical pulses on the same side of the original optical carrier pulse overlap with each other in the time domain, but have different phases. After the optical-to-electrical conversion at the PD, the output electrical signal is as follows

$$I_{\text{out}}(z,t)=2\gamma^2 J_1^2(\beta)\exp\left[-\frac{\left(t+\omega_{\text{RF}}\beta_2 z\right)^2}{T_0^2}\right]\left[1+\cos(\varphi-\psi)\right] \quad (9)$$
$$+2\gamma^2 J_1^2(\beta)\exp\left[-\frac{\left(t-\omega_{\text{RF}}\beta_2 z\right)^2}{T_0^2}\right]\left[1+\cos(\varphi+\psi)\right]$$

It can be seen that the output of the PD contains two pulses after AOA-to-power and frequency-to-time mapping. The diagram of simultaneous AOA-to-power and frequency-to-time mapping is shown in Fig. 2. It can be seen that the AOA-dependent phase difference φ and the angular frequency ω_{RF} of the received RF signals are simultaneously mapped into the amplitude $A_{\pm}$ and the time interval Δt of the output electrical signal, respectively. By extracting the amplitudes of the left and right pulses and the time interval between them, the AOA and the frequency of the RF signals can be obtained.

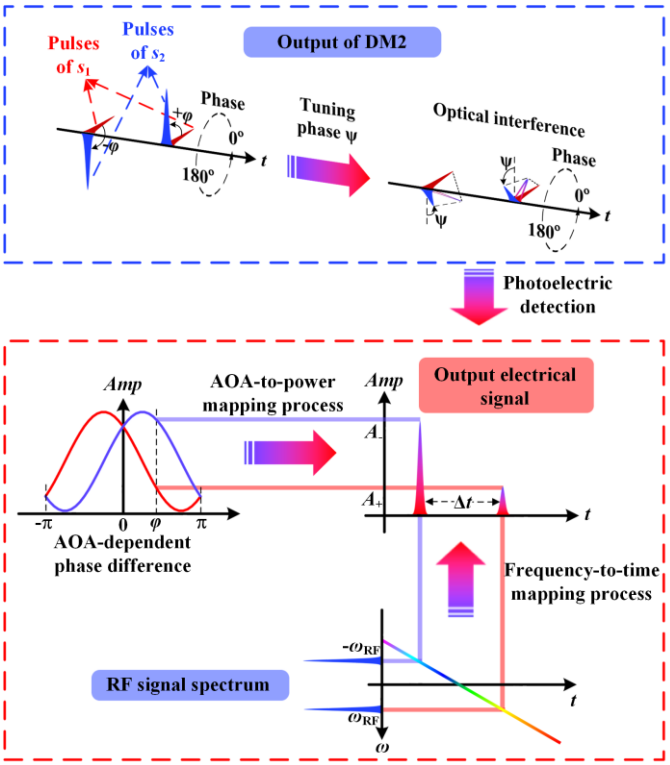

Fig. 2. Diagram of the simultaneous AOA-to-power and frequency-to-time mapping, showing the relationship between the output waveform and the frequency and the AOA-dependent phase difference of the modulated microwave signal.

The time interval between the two output electrical pulses can be expressed as

$$\Delta t=2\omega_{\text{RF}}\beta_2 z \quad (10)$$

Hence, the angular frequency of the received RF signals ω_{RF} can be easily calculated from the time interval Δt and the 2nd dispersion value $\beta_2 z$, with the expression as follows

$$\omega_{\text{RF}}=\frac{\Delta t}{2\beta_2 z} \quad (11)$$

It is noteworthy that the proposed structure enables a single-shot frequency measurement with a single optical pulse generated from the MLL. The time taken for a single measurement is decided by $1/f_{\text{MLL}}$, where f_{MLL} is the pulse repetition frequency of the MLL. Assuming that f_{MLL} is higher than 10 MHz, the frequency measurement rate can be higher than 10^7 times per second.

In addition, the phase difference φ between the two received RF signals can be obtained from the amplitudes of the left and right pulses. The normalized amplitudes of the left and right output pulses can be expressed as follows

$$\begin{cases}\dfrac{A_-(\varphi)}{A_{-,\max}}=\dfrac{1+\cos(\varphi-\psi)}{2}\\[2ex]\dfrac{A_+(\varphi)}{A_{+,\max}}=\dfrac{1+\cos(\varphi+\psi)}{2}\end{cases} \quad (12)$$

where $A_{-,\max}=A_-(-\psi+2k\pi)$ and $A_{+,\max}=A_+(\psi+2k\pi)$ (k=-1, 0, 1, ⋯) are the maximum amplitudes of the output left and right pulses, respectively. As can be seen, the normalized amplitudes vary as cosine-shape with φ. The values of φ calculated from the two normalized amplitudes are as follows

$$\begin{cases}\varphi_-=\arccos\left(\dfrac{2A_-(\varphi)}{A_{-,\max}}-1\right)+\psi\\[2ex]\varphi_+=\arccos\left(\dfrac{2A_+(\varphi)}{A_{+,\max}}-1\right)-\psi\end{cases} \quad (13)$$

The range of values for φ_- and φ_+ is [-π, π]. The AOA of θ can be calculated by the same solution in φ_- and φ_+. In this way, the ambiguous solution for φ will be removed. The solution for θ can be expressed as follows

$$\theta=\arcsin\left[\frac{\left(\varphi_-\cap\varphi_+\right)}{\pi}\right] \quad (14)$$

A single-shot AOA measurement is also taken based on a single optical pulse generated by the MLL, guaranteeing the high-speed measurement with the AOA. In addition, when receiving multiple RF signals with different frequencies, the output signals from the PD are as follows

$$I_{\text{multi}}(z,t)\propto\sum_{i=1}^{N}\left\{\exp\left[-\frac{\left(t+\omega_{\text{RF},i}\beta_2 z\right)^2}{T_0^2}\right]\left[1+\cos(\varphi_i-\psi)\right]\right. \quad (15)$$
$$\left.+\exp\left[-\frac{\left(t-\omega_{\text{RF},i}\beta_2 z\right)^2}{T_0^2}\right]\left[1+\cos(\varphi_i+\psi)\right]\right\}$$

where N is the amount of the received RF signals. As can be seen, the different frequencies are mapped into the different time intervals of the output pulses. The pulses carrying different frequency information are independent of each other in the time domain and can be measured individually. Therefore, the proposed structure can realize simultaneous AOA and frequency measurement of multiple signals.

III. Simulation

To verify the principle of the proposed system, the

simulations are firstly performed based on the scheme shown in Fig. 1. The FWHM of the optical pulse is set to be 700 fs, and the 2nd dispersion values of the LCFBGs are set to be ±2000 ps/nm, respectively. Single-frequency signals from 4 to 18 GHz with a step of 2 GHz are set as the signals under test (SUTs). The simulated output electrical pulses are shown in Figs. 3 (a)-(d), when the AOA-dependent phase differences between the RF signals received by RA1 and RA2 are -180º, -90º, 0º, and 90 º, respectively.

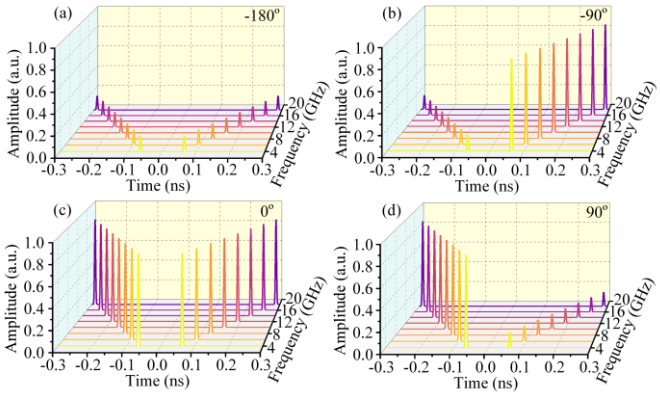

Fig. 3. The simulated results of the output electrical pulses when the frequencies of the received RF signal are 4-18 GHz with a 2-GHz step and the AOA-dependent phase differences are (a) -180º, (b) -90 º, (c) 0º, (d) 90º.

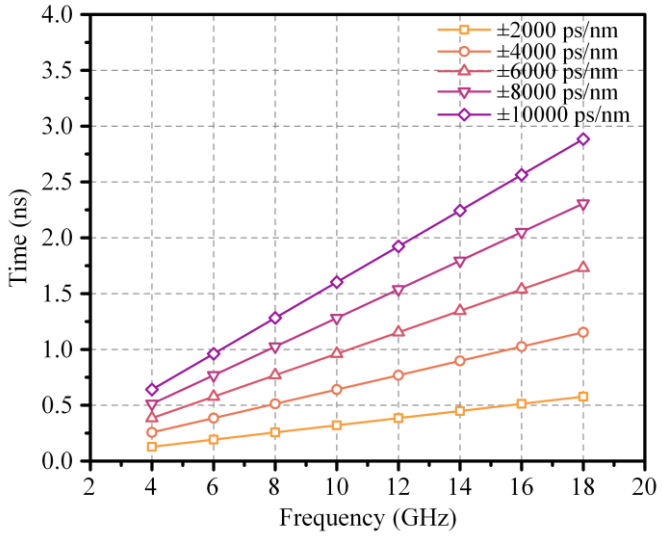

Fig. 4. The simulated curves of the time interval between the output pulses as a function of the frequency of the received RF signal under different 2nd dispersion values.

The simulated results show that the time interval of the output electrical pulses is positively correlated with the frequency of the SUT. Moreover, the amplitudes of the output electrical pulses are fluctuant with the AOA-dependent phase differences. Fig. 4 shows the simulated curves of the time intervals between the output pulses as a function of the frequency of the received RF signal, when the 2nd dispersion values of the LCFBGs are set from ±2000 to ±10000 ps/nm. It can be seen that the time interval of output pulses is linearly related to the frequency of the received RF signal. Furthermore, combined with Eq. (10), it is not difficult to find that the time interval is proportional to the 2nd dispersion values. Keeping the repetition frequency and the FWHM of the optical pulse unchanged, the larger the 2nd dispersion values are, the higher the frequency resolution is, but the smaller the frequency measurement range is. Therefore, the frequency of the received RF signal can be estimated by measuring the time interval of the output pulses.

To further investigate the effect of the additional phase introduced by MZM-c with the AOA measurement, MZM-c is biased at four different transmission points: the minimum, quadrature+, maximum, and quadrature- transmission points, respectively. The AOA-dependent phase differences of the SUT are from -180º to 180º and the frequency of the SUT is 10 GHz. The curves of the output pulse amplitudes versus the AOA-dependent phase difference corresponding to different biasing points with MZM-c are shown in Fig. 5. The blue and red curves in Fig. 5 represent the left and right pulses amplitudes, respectively. As can be seen, for all four biasing conditions with MZM-c, the curves have the cosine-shape, but the relative location of the curves corresponding to the left and right pulses amplitudes are different. When MZM-c is biased at the minimum or maximum transmission points, as shown in Fig. 5 (a) and Fig. 5 (c), the AOA-dependent phase difference solution is not unique. For example, the phase differences of $-\varphi$ and $+\varphi$ can be calculated from one amplitude value in Fig. 5 (a), the phase differences of $\mathrm{sgn}(\varphi)\times180^{o}-\varphi$ and φ can be calculated from one amplitude value in Fig. 5 (c). Thus, for these two conditions, there is only a 180º unambiguous AOA-dependent phase difference measurement range.

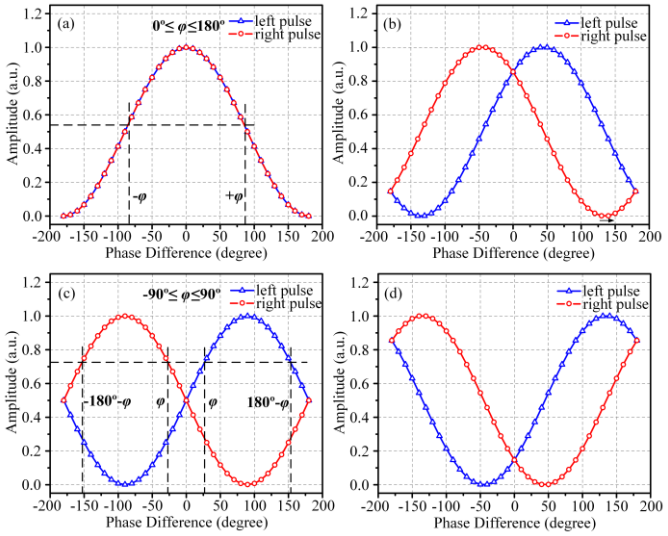

Fig. 5. The simulated amplitude curves of the output pulses when MZM-c is biased at the (a) minimum, (b) quadrature+, (c) maximum, (d) quadrature-transmission points.

When MZM-c is biased at the quadrature+ or the quadrature-transmission points, the AOA-dependent phase differences are one-to-one mapped to the pulse amplitudes, as shown in Fig 5 (b) and Fig. 5 (d), respectively. It can be seen that the AOA measurement ambiguity is eliminated, and the unambiguous AOA-dependent phase difference measurement range can cover 360º. In addition, the best phase difference measurement accuracy will be obtained at the steepest gradient descent or

boosting positions of the amplitude curves, while the worst one will be obtained at the peak or valley positions of the amplitude curves. As shown in Fig. 5 (b) and Fig. 5 (d), the peak or valley position of one amplitude curve corresponds to the steepest gradient descent or boosting position of the other curve. Thus, when MZM-c is biased at the quadrature transmission points, the overall phase difference measurement accuracy is optimal.

IV. Experimental Results

Based on the schematic diagram in Fig. 1, a proof-of-concept experiment is taken. The experimental setup is illustrated in Fig. 6. The ultrafast optical pulse with an FWHM of 150 fs, a repeat frequency of 100 MHz, and a center wavelength of 1560 nm is generated by an MLL (MenloSystems ELMO-780). In the experiment, to make the frequency spectrum range of the optical pulses satisfy the frequency response range of LCFBGs, an optical tunable filter (OTF, Santec OTF-980) is applied to select the spectrum range of the optical pulses. Two LCFBGs with the 2nd dispersion values of ±10000 ps/nm are used as DM1 and DM2, respectively. A DPMZM (Fujitsu FTM7961EX) with a half-wave voltage of 3.5 V and a working bandwidth of 40 GHz is used. An erbium-doped fiber amplifier (EDFA, Amonics AEDFA-PA-35-R-FA) is inserted to compensate the optical link loss. The PD (Finisar XPDV2120R-VF-FP) has a 50-GHz working bandwidth and a 0.6-A/W responsivity. An arbitrary waveform generator (AWG, Keysight M8195A) with two output channels and a maximum sample rate of 65 GSa/s is used to generate the RF signals to be measured. The output electronic pulses are observed by a real-time oscilloscope (Tektronix DSA72004B) with a maximum sample rate of 50 GSa/s. It should be noted that the maximum frequency of the RF signal set in the experiment is 15GHz, so the distance *d* of two receive antennas is assumed to be 1 cm to achieve unambiguous AOA measurement.

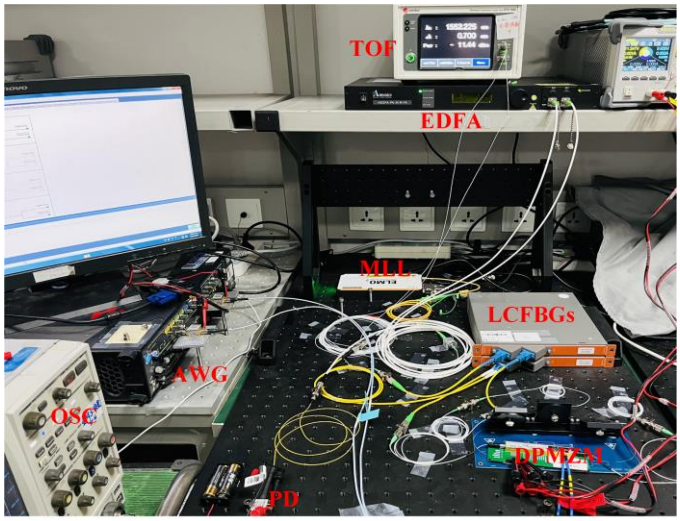

Fig. 6. The illustration of the experimental setup. MLL: mode-lock laser; TOF: tunable optical filter; EDFA: erbium-doped fiber amplifier; LCFBGs: linear chirped fiber Bragg gratings; DPMZM: dual-parallel Mach-Zehnder modulator; PD: photodetector; AWG: arbitrary waveform generator; OSC: oscilloscope.

A. AOA and Frequency Measurement

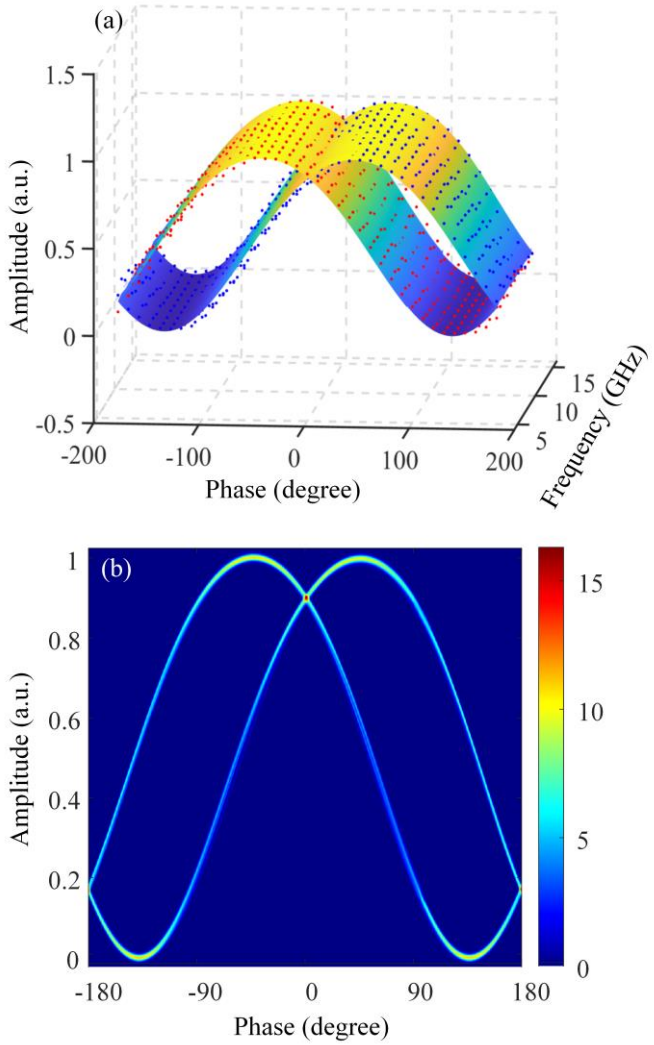

Fig. 7. (a) The experimentally obtained fitted normalized amplitudes surfaces of the output left and right pulses when the frequencies of the received RF signals are from 5 to 15 GHz and the AOA-dependent phase differences are from -180º to 180º. (b) The projections of the two fitted surfaces on the phase-amplitude plane.

To investigate the AOA and frequency measurement capabilities, the experiments were firstly carried out with the single-tone RF signals measurement. Two RF signals with the same frequency and different phases are generated from two channels of the AWG as the received RF signals. The phase difference between the two RF signals is tuned from -180º to 180º with a step of 10º. The frequency of the two RF signals is tuned from 5 to 15 GHz with a step of 1 GHz. The experimental results of AOA measurement are shown in Fig. 7. The blue and red dots in Fig. 7 (a) indicate the normalized amplitudes of the output left and right pulses, respectively. Two phase-frequency-amplitude surfaces are obtained by fitting the dots through the Levenberg-Marquardt algorithm (LMA) [33]. The projections of the two fitted surfaces on the phase-amplitude plane are given in Fig. 7 (b). It shows a good agreement between the experimental results and the simulation results in Fig 5. (b) .

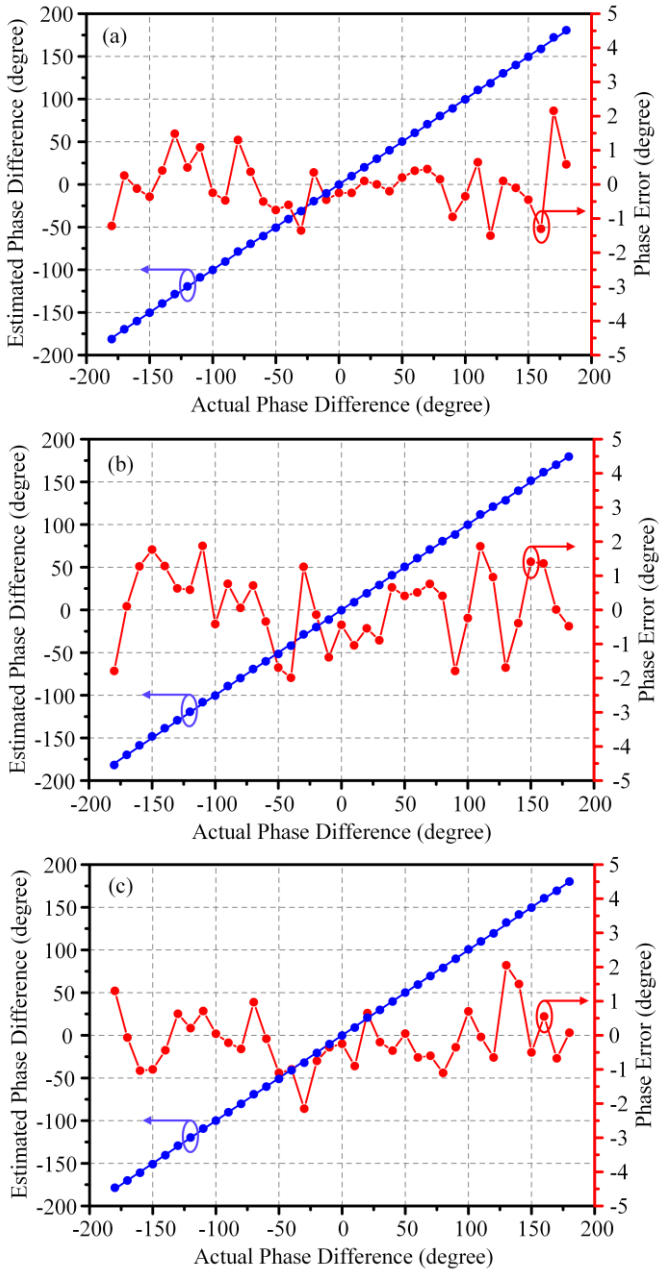

Fig. 8. The relationship between the measured and the actual AOA-dependent phase differences (blue dotted line), and the estimation errors (red dotted line), when the frequencies of the received RF signals are (a) 8, (b) 10, and (c) 12 GHz.

To investigate the AOA measurement performance of the proposed system, single-tone RF signals with frequencies of 8, 10, and 12 GHz are measured, for which the AOA-dependent phase differences are tuned from -180º to 180º with a step of 10º. The AOA-dependent phase difference is estimated by comparing the normalized amplitudes of the output left and right pulses. The blue dots in Fig. 8 are the experimentally measured results of AOA-dependent phase differences, while the blue lines represent the ideal estimation without errors. In addition, the estimation errors at different frequencies are shown as the red dots. It can be seen that for the RF signals with frequencies of 8, 10 and 12 GHz, the estimation errors for the AOA-dependent phase difference are within ±2.16º, ±1.88º and ±2.15º, respectively.

Based on Eq. (14), there is a nonlinear mapping relationship between the AOA and the AOA-dependent phase difference. The simulated mapping curves between the AOA and the AOA-dependent phase difference are shown in Fig. 9, for the frequency range of 5-15 GHz. As can be seen that the nonlinear mapping curves are frequency-dependent. The slopes of all the mapping curves are close to ∞ as the AOA approaches ±90º. This means that a slight measurement error of the AOA-dependent phase difference will lead to a large AOA estimation error when the AOA is close to ±90º.

In the experiment, to guarantee the AOA measurement accuracy, the measurement range of the AOA is selected to be -70º to 70º. By mapping the experimentally estimated results of the AOA-dependent phase difference in Figs. 8 (a)-(c) to the AOA, the AOA estimation errors are shown in Fig. 10. It can be seen that the AOA measurement from -70º to 70º is successfully achieved, with the AOA estimation error within ±2.5º. When the AOA is close to the boundary values (-70º and 70º), the AOA measurement accuracy deteriorates significantly.

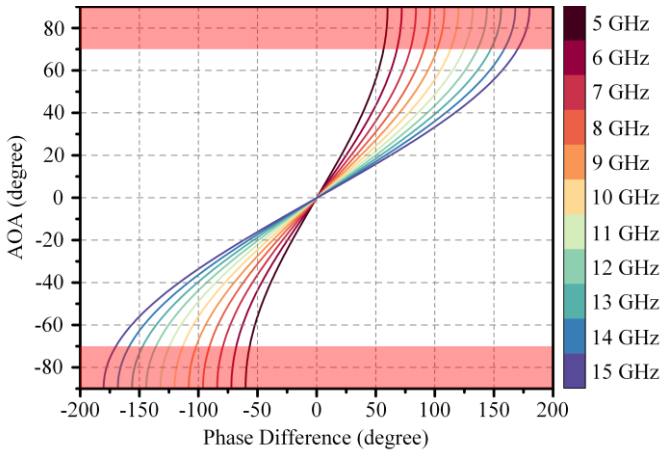

Fig. 9. The simulated mapping curves between the AOA and the AOA-dependent phase difference, when the frequency of the received signal is from 5-15 GHz with a 1-GHz step.

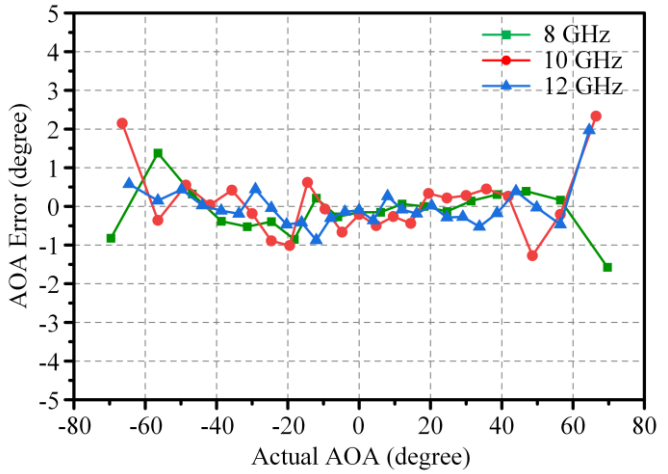

Fig. 10. The AOA estimation errors, when the frequencies of the received signals are 8 GHz, 10 GHz, and 12 GHz.

Fig. 11 shows the experimental frequency measurement results. The single-tone RF signals are tuned from 5 to 15 GHz

with a 1-GHz step. The blue and red solid lines in Fig. 11 (a) indicate the experimentally fitted frequency-to-time mapping curves, when the AOA-dependent phase differences are set to be -45º and 0º, respectively. As can be seen, the frequency of the received RF signals is linearly related to the time interval of the output electrical pulses, which agrees well with the theoretical analyses and simulations. The slopes of the frequency-to-time mapping curves are measured to be 6.2344 GHz/ns for both conditions.

The dash lines in Fig. 11 (a) represent the mean frequency estimation errors, which are within ±12 MHz. The insets of Figs. 11 (b) and (c) indicate the experimentally obtained time-domain waveforms of the output pulses when the frequencies of the received RF signals are 6 and 14 GHz, respectively. As can be seen, the frequency and the AOA measurement can be achieved within one repetition period of the optical pulses generated from the MLL. Thus, the frequency measurement within 5-15 GHz is successfully experimentally realized for different AOA conditions.

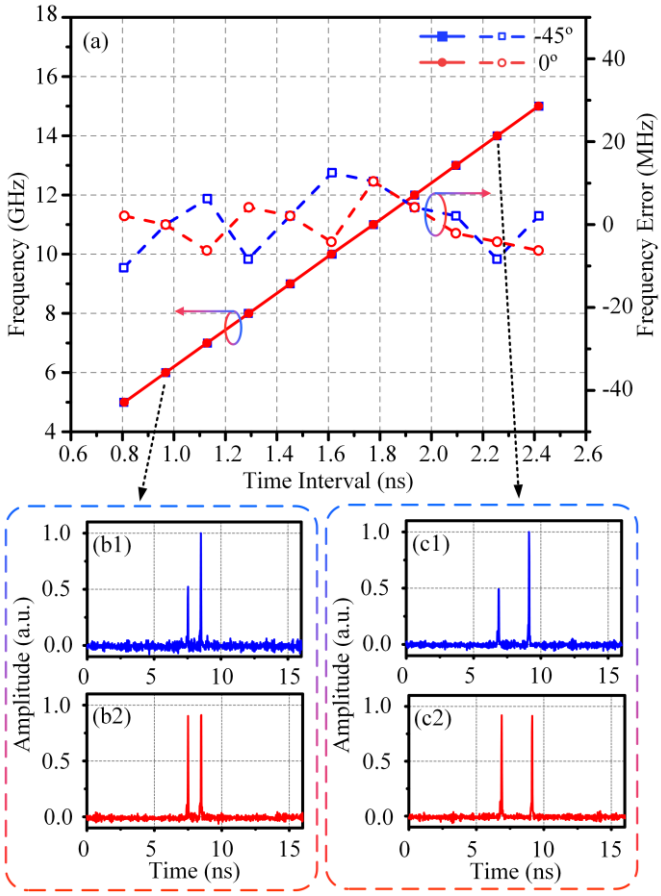

Fig. 11. (a) The fitted curves of the experimentally measured frequency values (solid lines) and the frequency estimation error (dash lines) versus the pulses time intervals, for the working frequency range of 5-15 GHz, when the AOA-dependent phase differences are -45º (blue) and 0º (red), respectively. The experimentally obtained time-domain waveforms of the output pulses when the RF signal frequencies are (b) 5 and (c) 14 GHz, and the AOA-dependent phase differences are (1) -45º and (2) 0º, respectively.

B. Multiple RF Signals Measurement

To demonstrate the multiple RF signals measurement capability of the proposed system, an experiment is taken to measure the AOA and the frequency of two RF signals. The actual parameters of the received RF signals are shown in Table I.

TABLE I
ACTUAL PARAMETERS OF THE RECEIVED MULTIPLE RF SIGNALS

Frequency	AOA-dependent phase difference	AOA
8.100 GHz	-50.00º	-30.96º
14.800 GHz	80.00º	26.77º

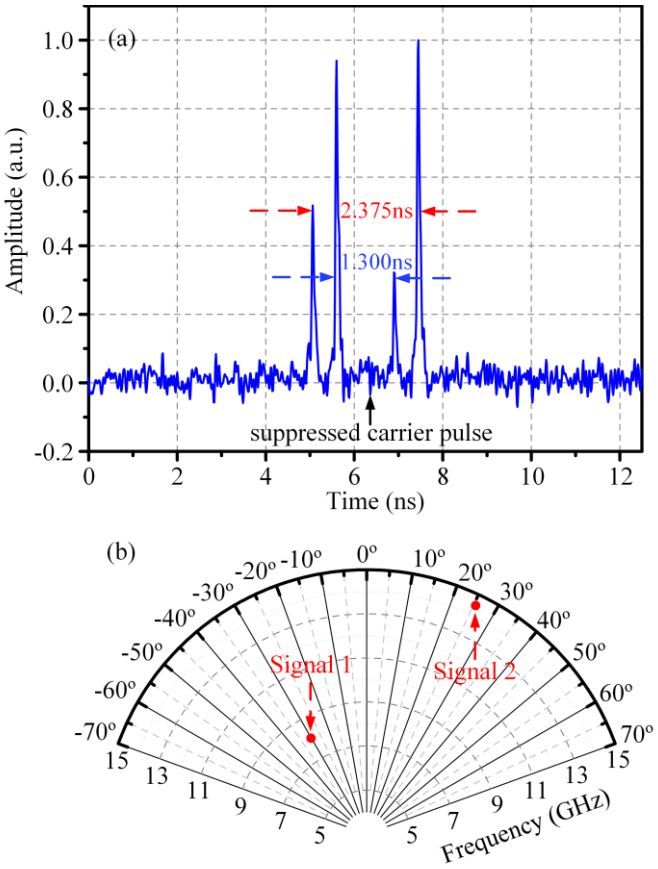

Fig. 12. (a) The experimentally obtained time-domain waveforms of the output pulses when receiving multiple RF signals with parameters shown in Table I. (b) The measured AOA and frequency distribution of the received RF signals.

TABLE II
ESTIMATED PARAMETERS OF THE RECEIVED MULTIPLE RF SIGNALS

Frequency	AOA-dependent phase difference	AOA
8.105 GHz	-49.70º	-30.73º
14.807 GHz	77.84º	25.98º

The experimentally obtained time-domain waveform of the output pulses in a single-shot measurement is shown in Fig. 12 (a). It can be seen that two pairs of pulses with different time intervals and different normalized amplitudes are contained. Based on Eq. (15), it can be known that the output electrical pulses are symmetrically distributed on both sides of the suppressed carrier pulse. Thus, time intervals can be obtained as 1.300 ns and 2.375 ns from Fig. 12 (a), respectively. The estimated parameters of the multiple RF signals based on the time-domain waveform in Fig. 12 (a) are shown in Table II. By comparing Table I and Table II, it can be seen that the frequency

TABLE III
THE COMPARISON WITH THE STATE-OF-ART AOA AND FREQUENCY MEASUREMENT SYSTEMS

Scheme	Simultaneous AOA and frequency measurement	AOA measurement range	AOA measurement error	Frequency measurement range
Microwave photonic down-conversion based on single LO signal [14]	Yes	-0º to 90º	±1º	Narrow-band (several MHz)
Microwave photonic down-conversion based on frequency-stepped LO signal [17]		-20º to 20º	±1.2º	8-12 GHz
Microwave photonic channelization [19]		-15º to 15º	⩽3.54º	16-20 GHz
Coherent optical processing [20]		-15º to 15º	⩽0.5º	12-18 GHz
AOA-to-power mapping based on DDMZM [28]	No	12.6º to 90º	⩽2.0º	Single frequency (prior information)
AOA-to-power mapping based on two-level signal controlled DDMZM [29]		-70.8º to 70.8º	±2.0º	Single frequency (prior information)
AOA-to-power mapping based on the parallel DDMZMs [31]		0º to 63º	⩽2.0º	Single frequency (prior information)
Simultaneous Frequency-to-time mapping and AOA-to-power mapping [this work]	Yes	-70º to 70º	±2.5º	5-15 GHz

estimation errors are 5 MHz and 7 MHz, and the AOA estimation errors are -0.23º and 0.79º for the two RF signals, respectively. Based on the measurement results in Table II, the AOA and frequency distribution of the received multiple RF signals can be obtained as shown in Fig. 12 (b). Thus, the simultaneous AOA and frequency measurement with multiple RF signals is experimentally achieved successfully. Table III shows the comparison between this work and the state-of-art AOA and frequency measurement systems. It can be seen that the proposed system has larger AOA and frequency measurement range, smaller measurement errors, and have the capability to simultaneously measure AOA and frequency for multiple RF signals.

In addition, the proposed scheme achieves the simultaneous AOA and frequency measurement with wide working ranges by constructing the AOA-to-power mapping link and the frequency-to-time mapping link simultaneously in a single optical link, avoiding the use of large-scale optical links. Thus, the requirement of devices, the complexity and the cost of the system are greatly reduced.

V. CONCLUSION

In conclusion, a simultaneous AOA and frequency measurement system based on microwave photonics is proposed and demonstrated experimentally. Based on phase-to-power and frequency-to-time mapping, simultaneous AOA and frequency measurement can be achieved within a wide range. The AOA measurement from -70º to 70º is experimentally achieved with a measurement error within ±2.5º, while the simultaneous frequency measurement from 5-15 GHz is achieved with a measurement error within ±12 MHz. The AOA and frequency measurement with multiple RF signals is also experimentally realized. It should be noted that the proposed system can only measure the horizontal AOA. By applying an L-shape antenna array [34] and a dual-polarization DPMZM, the AOA in both horizontal and vertical directions will be measured simultaneously. The proposed scheme can find applications in wireless communication, radar and electronic warfare systems.

REFERENCES

[1] V. Teppati, A. Ferrero, and M. Sayed, *Modern RF and microwave measurement techniques*. Cambridge University Press, 2013.

[2] D. Zhu and S. L. Pan, "Broadband cognitive radio enabled by photonics," *J. Lightw. Technol.*, vol. 38, no. 12, pp. 3076-3088, May. 2020.

[3] A. E. Spezio, "Electronic warfare systems," in *IEEE Trans. Microw. Theory Technol.*, vol. 50, no. 3, pp. 633-644, Mar. 2002.

[4] M. Li and Y. Lu, "Angle-of-arrival estimation for localization and communication in wireless networks," in *16th European Signal Processing Conference (EUSIPCO)*, 2008, pp. 1-5.

[5] E. Mosca, "Angle estimation in amplitude comparison monopulse systems," *IEEE Aerosp. Electron. Syst.*, vol. 2, pp. 205-212, 1969.

[6] L. Cong and W. Zhuang, "Hybrid TDOA/AOA mobile user location for wideband CDMA cellular systems," *IEEE Trans. Wirel. Commun.*, vol. 1, no. 3, pp. 439-447, Jul. 2002.

[7] N. Iwakiri and T. Kobayashi, "Ultra-Wideband Time-of-Arrival and Angle-of-Arrival Estimation Using Transformation Between Frequency and Time Domain Signals," *J. Commun.*, vol. 1, no. 3, pp. 12-19, Jan. 2008.

[8] J. Yao, "Microwave Photonics," *J. Lightw. Technol.*, vol. 27, no. 3, pp. 314–335, Feb. 2009.

[9] X. Zou, B. Lu, W. Pan, L. Yan, A. Stöhr, and J. Yao, "Photonics for microwave measurements," *Laser Photonics Rev.*, vol. 10, no. 5, pp. 711-734, Jul. 2016.

[10] J. Capmany and D. Novak, "Microwave photonics combines two worlds," *Nat. Photonics*, vol. 1, no. 6, pp. 319–330, Jun. 2007.

[11] C. Huang and E. H. W. Chan, "Multichannel microwave photonic based direction finding system," *Opt. Express*, vol. 28, no. 17, pp. 25346-25357, Aug. 2020.

[12] P. Li, L. Yan, J. Ye, X. Feng, W. Pan, B. Luo, and Z. Chen, "Photonic approach for simultaneous measurements of Doppler-frequency-shift and angle-of-arrival of microwave signals," *Opt. Express*, vol. 27, no. 6, pp. 8709-8716, Mar. 2019.

[13] Z. Zhang, M. Chen, Q. Guo, H. Chen, S. Yang, and S. Xie, "Photonic mixing approach to measure the angle-of-arrival of microwave signals," in *2016 Conference on Lasers and Electro-Optics (CLEO)*, 2016, pp. 1-2.

[14] C. Huang, H. Chen, and E. H. W. Chan, "Simple photonics-based system for Doppler frequency shift and angle of arrival measurement," *Opt. Express*, vol. 28, no. 9, pp. 14028-14037, Apr. 2020.

[15] Z. Tang and S. Pan, "Simultaneous measurement of Doppler-frequency-shift and angle-of-arrival of microwave signals for automotive radars," in *2019 International Topical Meeting on Microwave Photonics (MWP)*, 2019, pp. 1-4.

[16] H. Zhuo and A. Wen, "A photonic approach for Doppler-frequency-shift and angle-of-arrival measurement without direction ambiguity," *J. Lightw. Technol.*, vol. 39, no. 6, pp. 1688-1695, Mar. 2020.
[17] Y. Yang, C. Ma, F. Zhang, B. Fan, X. Wang, and S. Pan, "Photonics-based simultaneous angle of arrival and frequency measurement for multiple targets detection," in *2020 International Topical Meeting on Microwave Photonics (MWP)*, 2020, pp. 14-17.
[18] Y. Yang, C. Ma, B. Fan, X. Wang, F. Zhang, Y. Xiang, and S. Pan, "Photonics-Based Simultaneous Angle of Arrival and Frequency Measurement System with Multiple-Target Detection Capability," *J. Lightw. Technol.*, vol. 39, no. 24, pp. 7656-7663, Jun. 2021.
[19] Y. Yang, J. Ding, C. Ma, F. Cao, X. Wang, and S. Pan, "Photonics-assisted Wideband RF Source Localization Method Based on Synthetic Aperture Interferometric Detection," *J. Lightw. Technol.*, vol. 40, no. 19, pp. 6366-6373, Oct. 2022.
[20] J. Murakowski, G. J. Schneider, S. Shi, C. A. Schuetz, and D. W. Prather, "Photonic probing of radio waves for k-space tomography," *Opt. Express*, vol. 25, no. 14, pp. 15746-15759, Jul. 2017.
[21] J. C. Deroba, G. J. Schneider, C. A. Schuetz, and D. W. Prather, "Multifunction radio frequency photonic array with beam-space down-converting receiver," *IEEE Aerosp. Electron. Syst.*, vol. 54, no. 6, pp. 2746-2761, Dec. 2018.
[22] H. Chen and E. H. W. Chan, "Angle-of-arrival measurement system using double RF modulation technique," *IEEE Photon. J.*, vol. 11, no. 1, pp. 1-10, Feb. 2018.
[23] X. Zou, W. Li, W. Pan, B. Luo, L. Yan, and J. Yao, "Photonic approach to the measurement of time-difference-of-arrival and angle-of-arrival of a microwave signal," *Opt. Lett.*, vol. 37, no. 4, pp. 755-757, Feb. 2012.
[24] X. Zou and J. Yao, "Microwave and millimeter-wave measurements using photonics," *SPIE Newsroom*, New York, NY, USA, pp. 1-3, Nov. 2015.
[25] Z. Cao, R. Lu, Q. Wang, A. C. F. Reniers, H. P. A. van den Boom, E. Tangdiongga, and A. M. J. Koonen, "Photonic Angle-of-arrival Measurement of a Microwave Signal with Range Selectivity and SNR Enhancement," arXiv preprint, to be published. DOI: 10.48550/arXiv.1311.4326.
[26] H. Zhuo, A. Wen, and Y. Wang, "Photonic angle-of-arrival measurement without direction ambiguity based on a dual-parallel Mach–Zehnder modulator," *Opt. Commun.*, vol. 451, pp. 286-289, Jun. 2019.
[27] Z. Cao, Q. Wang, R. Lu, H. P. A. van den Boom, E. Tangdiongga, and A. M. J. Koonen, "Phase modulation parallel optical delay detector for microwave angle-of-arrival measurement with accuracy monitored," *Opt. Lett.*, vol. 39, no. 6, pp. 1497-1500, Mar. 2014.
[28] H. Chen and E. H. W. Chan, "Simple approach to measure angle of arrival of a microwave signal," *IEEE Photon. Technol. Lett.*, vol. 31, no. 22, pp. 1795-1798, Nov. 2019.
[29] G. Li, D. Shi, L. Wang, Y. Xiao, M. Li, N. Zhu, and W. Li, "Unambiguous measurement of AOA using a DDMZM," *Opt. Commun.*, vol. 514, pp. 128-132. Feb. 2022.
[30] H. Chen and E. H. W. Chan, "Technique to eliminate RF signal amplitude dependence in AOA measurement," *Electron. Lett.*, vol. 56, no. 5, pp. 243-244, Apr. 2020.
[31] H. Chen and E. H. W. Chan, "Photonics-based CW/pulsed microwave signal AOA measurement system," *J. Lightw. Technol.*, vol. 38, no. 8, pp. 2292-2298, Apr. 2020.
[32] G. P. Agrawal, *Nonlinear fiber optics*. Springer, Berlin, Heidelberg, 2000, pp. 195-211.
[33] J. J. Moré, "The Levenberg-Marquardt algorithm: implementation and theory," *Numerical analysis*, Springer, Berlin, Heidelberg, pp. 105-116, 1978.
[34] N. Tayem and H. M. Kwon, "L-shape 2-dimensional arrival angle estimation with propagator method," *IEEE Trans. Antennas Propag.*, vol. 53, no. 5, pp. 1622-1630, May. 2005.

Jiewen Ding (Student Member, IEEE) received B.S. degree in electronic science and technology in 2019 from Nanjing University of Aeronautics and Astronautics, Nanjing, China, where he is currently working toward the M.S. degree. His research focuses on microwave photonic processing.

Dan Zhu (Member, IEEE) received the B.S. and Ph.D. degrees in electronic engineering from Tsinghua University, Beijing, China, in 2004 and 2009, respectively. In May 2011, she joined the College of Electronic and Information Engineering, Nanjing University of Aeronautics and Astronautics, Nanjing, China, where she is currently a Professor. From May 2014 to May 2015, she was a Visiting Scholar at the Microwave Photonics Research Laboratory, University of Ottawa, Canada. Her current research interests include microwave photonic signal processing and the system applications.

Prof. Zhu is a member of the IEEE Microwave Theory and Techniques Society, the IEEE Photonics Society, and the Optical Society of America.

Boyang Ni received the B.S. degree in communication engineering in 2022 from Nanjing University of Aeronautics and Astronautics, Nanjing, China, where he is currently working toward the M.S. degree. His research focuses on microwave photonic processing.

Chao Zhang received the B.S. degree in communication engineering in 2021 from Anhui Agricultural University, China, where he is currently working toward the M.S. degree. His research focuses on microwave photonic processing.

Shilong Pan (Senior Member, IEEE) received the B.S. and Ph.D. degrees in electronic engineering from Tsinghua University, Beijing, China, in 2004 and 2008, respectively. From 2008 to 2010, he was a "Vision 2010" Postdoctoral Research Fellow with the Microwave Photonics Research Laboratory, University of Ottawa, Canada. In 2010, he joined the College of Electronic and Information Engineering, Nanjing University of Aeronautics and Astronautics, China, where he is currently a Full Professor and an Executive Director of the Key Laboratory of Radar Imaging and Microwave Photonics, Ministry of Education.

His research focused on microwave photonics, which includes optical generation and processing of microwave signals, analog photonic links, photonic microwave measurement, and integrated microwave photonics.

Prof. Pan is currently an Associate Editor for *Electronics Letters*, a Topical Editor of *Chinese Optics Letters*, and is a Technical Committee Member of IEEE MTT-3 Microwave Photonics. He was also a Chair of a number of international conferences, symposia, and workshops, including the TPC Chair of the International Conference on Optical Communications and Networks in 2015, and TPC Co-Chair of the IEEE International Topical Meeting on Microwave Photonics in 2017. He is a Fellow of OSA, SPIE, and IET. He was selected as an IEEE Photonics Society Distinguished Lecturer in 2019.